

FastDSAC: Unlocking the Potential of Maximum Entropy RL in High-Dimensional Humanoid Control

Jun Xue^{1,2} Junze Wang^{1,3} Xinming Zhang¹ Shanze Wang¹ Yanjun Chen¹ Wei Zhang¹

Abstract

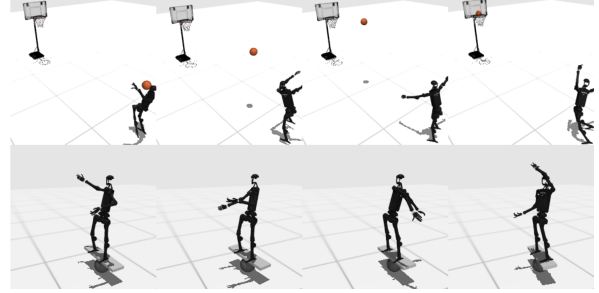
Scaling Maximum Entropy Reinforcement Learning (RL) to high-dimensional humanoid control remains a formidable challenge, as the “curse of dimensionality” induces severe exploration inefficiency and training instability in expansive action spaces. Consequently, recent high-throughput paradigms have largely converged on deterministic policy gradients combined with massive parallel simulation. We challenge this compromise with FastDSAC, a framework that effectively unlocks the potential of maximum entropy stochastic policies for complex continuous control. We introduce Dimension-wise Entropy Modulation (DEM) to dynamically redistribute the exploration budget and enforce diversity, alongside a continuous distributional critic tailored to ensure value fidelity and mitigate high-dimensional value overestimation. Extensive evaluations on HumanoidBench and other continuous control tasks demonstrate that rigorously designed stochastic policies can consistently match or outperform deterministic baselines, achieving notable gains of 180% and 400% on the challenging *Basketball* and *Balance Hard* tasks.

1. Introduction

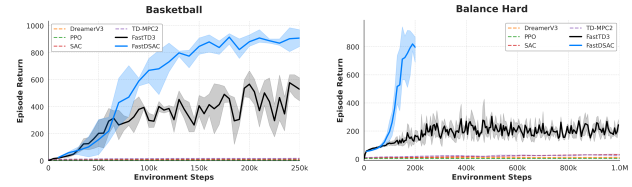
Deep reinforcement learning (RL) has driven significant progress in high-dimensional robotics, establishing itself as a cornerstone for acquiring versatile sensorimotor skills in humanoid control (Hansen et al., 2024; Hafner et al., 2023; Sferrazza et al., 2024; Zhuang et al., 2025; Seo et al., 2025b). As morphological complexity and task demands increase,

^{*}Equal contribution ¹the College of Information Science and Technology, Eastern Institute of Technology, Ningbo, China ²Department of Control Science and Engineering, Tongji University, Shanghai, China ³College of Computer Science and Technology, China University of Petroleum(East China), Qingdao, China. Correspondence to: Wei Zhang <zhw@eitech.edu.cn>.

Preprint. March 16, 2026.



(a) Visualization of FastDSAC’s performance on tasks



(b) Basketball

(c) Balance Hard

Figure 1. Performance of FastDSAC on high-dimensional humanoid control tasks. (a) Visualizations of the challenging *Basketball* and *Balance Hard* environments. (b, c) Evaluation curves comparing FastDSAC with the FastTD3 baseline. FastDSAC significantly outperforms FastTD3, achieving final returns 1.8× and 4.0× higher on the respective tasks with superior sample efficiency.

the field has shifted towards leveraging massively parallel simulation to accelerate training (Rudin et al., 2022; Kaufmann et al., 2023; Li et al., 2023; Shukla, 2025; Gallici et al., 2025). In this high-throughput setting, deterministic policy gradient methods, notably TD3 (Fujimoto et al., 2018) and its optimized variant FastTD3 (Seo et al., 2025b), have become the dominant choice for state-of-the-art (SOTA) performance. By leveraging the stability of deterministic policies in massively parallelized environments, such as IsaacLab (Mittal et al., 2023), MuJoCo Playground (Zakka et al., 2025), and HumanoidBench (Sferrazza et al., 2024), these approaches have successfully solved challenging locomotion and manipulation tasks that were once intractable.

Despite the dominance of deterministic methods, maximum entropy RL algorithms (e.g., SAC (Haarnoja et al., 2018)), theoretically offer compelling advantages, particularly in escaping local optima and fostering diverse behaviors, which are often absent in deterministic approaches. However, realizing these benefits in high-dimensional humanoid control is impeded by the “curse of dimensionality” (Köppen, 2000).

A primary obstacle is the presence of redundant actuators in complex robotic systems, where unconstrained exploration squanders the sample budget on task-irrelevant dimensions with minimal impact on the reward (Zhang & Cai, 2024). Furthermore, standard diagonal Gaussian policies, lacking structural prioritization or constraint, indiscriminately distribute exploration effort across this expanded volume ($|\mathcal{A}| > 20$). This inefficiency leads to a collapse of effective physical coverage, termed “vanishing exploration” (Schumacher et al., 2023; Wei et al., 2026). Consequently, absent a mechanism to selectively allocate exploration variance or enforce structural prioritization, stochastic agents frequently suffer from training instability and suboptimal convergence, a limitation persistently observed in recent SOTA baselines (Sferrazza et al., 2024; Seo et al., 2025b; Obando-Ceron et al., 2025; Wei et al., 2026).

Compounding the exploration difficulty is the inherent susceptibility of critic networks to severe value overestimation in high-dimensional action spaces. As the action space expands, critics are frequently queried on state-action pairs lying far from the training distribution (OOD). In these sparse regions, neural approximations suffer from severe extrapolation error, generating spurious Q-value spikes (Bhatt et al., 2019; Neumann et al., 2024). This issue is exacerbated in high-dimensional settings where the policy tends to over-exploit these approximation artifacts, aggressively shifting towards regions where the critic erroneously predicts high returns (Seo & Abbeel, 2025). Crucially, standard mitigation strategies, such as clipped double Q-learning, are often insufficient to suppress this overestimation bias in complex dynamics (Kuznetsov et al., 2020; Duan et al., 2020). Even recent parallelized approaches, utilizing either standard architectures or discrete distributional critics (Obando-Ceron et al., 2025; Shukla, 2025), struggle to resolve this instability, leading to suboptimal convergence. Compounding the general challenge of overestimation, discrete critics introduce inevitable quantization errors that distort the return distribution, further compromising the value fidelity required for high-precision control. This underscores the necessity of a continuous distributional critic, serving as a robust mechanism to simultaneously eliminate quantization artifacts and mitigate overestimation in high-throughput settings (Duan et al., 2025).

To bridge these gaps, we introduce FastDSAC, a framework that effectively scales maximum entropy stochastic policies to high-dimensional continuous control. FastDSAC integrates two core mechanisms to unlock the scalability and stability of learning in high-dimensional regimes. First, we propose Dimension-wise Entropy Modulation (DEM), which empowers the agent to autonomously redistribute the exploration budget across action dimensions. By effectively pruning the exploration subspace to suppress task-irrelevant noise, DEM avoids the structural inefficiency

of uniform exploration typical of standard policies. Second, we incorporate a continuous distributional critic parameterized by a Gaussian distribution (Duan et al., 2025). Distinct from baselines constrained by discrete approximations or deterministic estimates, this component enables precise continuous modeling of the full return distribution, thereby robustly mitigating the value overestimation driven by high-dimensional extrapolation errors. Extensive empirical evaluations on HumanoidBench, MuJoCo Playground, and IsaacLab confirm that FastDSAC consistently matches or surpasses SOTA baselines across the vast majority of evaluated tasks. Notably, it yields performance gains of approximately **180%** and **400%** over FastTD3 on the challenging *Basketball* and *Balance Hard* tasks, respectively, demonstrating that rigorously designed stochastic policies can achieve superior performance in high-dimensional robotics. An anonymous implementation of our method is provided at https://anonymous.4open.science/r/FastDSAC_ICML-5194.

2. Preliminaries

We formulate the continuous control problem as a Markov Decision Process (MDP), defined by the tuple $(\mathcal{S}, \mathcal{A}, p, r, \gamma)$, comprising the state space \mathcal{S} , action space \mathcal{A} , transition dynamics $p(s'|s, a)$, reward function $r(s, a)$, and discount factor $\gamma \in [0, 1)$. Our approach integrates two reinforcement learning paradigms:

Maximum Entropy Reinforcement Learning. To encourage robust exploration, we adopt the maximum entropy framework (Haarnoja et al., 2018). Instead of maximizing the scalar cumulative return, the agent learns a policy $\pi(\cdot|s)$ that maximizes the expected return augmented by an entropy term:

$$J(\pi) = \mathbb{E}_{\pi} \left[\sum_{t=0}^{\infty} \gamma^t \left(r(s_t, a_t) + \alpha \mathcal{H}(\pi(\cdot|s_t)) \right) \right], \quad (1)$$

where $\mathcal{H}(\pi(\cdot|s_t))$ is the entropy of the policy and α is a temperature parameter balancing reward and exploration.

Distributional Reinforcement Learning. Unlike standard methods that estimate the expected value $Q^{\pi}(s, a) = \mathbb{E}[Z^{\pi}(s, a)]$, we model the full distribution of the random return $Z^{\pi}(s, a)$. This distribution follows the distributional Bellman equation:

$$Z^{\pi}(s, a) \stackrel{D}{=} r(s, a) + \gamma Z^{\pi}(s', a'), \quad (2)$$

where $s' \sim p(\cdot|s, a)$, $a' \sim \pi(\cdot|s')$, and $\stackrel{D}{=}$ denotes equality in distribution. Capturing the full return distribution enables the agent to utilize higher-order moments (e.g., variance) for more stable learning signals.

2.1. Fast Actor-Critic (FastTD3)

Our work builds upon the architectural principles of FastTD3 (Seo et al., 2025b), an architecture designed for massive parallelism. It achieves high throughput via two core mechanisms:

- **Parallelized Data Collection:** Instead of a single replay buffer, FastTD3 leverages thousands of parallel environments to collect uncorrelated experiences per batch. This effectively mitigates the exploration capability issues often faced by deterministic policies, as the high volume of diverse samples compensates for local noise.
- **Categorical Value Estimation (C51):** FastTD3 approximates the return distribution using the Categorical Distribution (C51) (Bellemare et al., 2017), defined over a discrete support of N fixed atoms $\{z_i\}_{i=1}^N$ spanning $[v_{\min}, v_{\max}]$. Target estimation employs the projected Bellman update $\mathbf{m} = \Phi \mathcal{T} Z_{\theta}$. Here, the distributional Bellman operator \mathcal{T} , first shifts the distribution via $r(s, a) + \gamma Z(s', a')$, and Φ subsequently projects the result onto the fixed atoms. The critic minimizes the Cross-Entropy loss between the predicted probability vector \mathbf{p} and the projected target \mathbf{m} :

$$\mathcal{L}_{\text{C51}}(\theta) = - \sum_{i=1}^N m_i \log p_i(s, a). \quad (3)$$

However, this reliance on fixed discretization introduces fundamental limitations: the inherent quantization errors restrict value estimation precision, particularly in continuous control tasks requiring fine-grained signal propagation.

2.2. Continuous Distributional Critics (DSAC)

To mitigate the quantization errors inherent in discrete distributional approximations, we employ the Discrete Soft Actor-Critic (DSAC) framework (Duan et al., 2020; 2025). DSAC parameterizes the return distribution as a continuous Gaussian $Z_{\theta}(\cdot|s, a) \sim \mathcal{N}(Q_{\theta}(s, a), \sigma_{\theta}^2(s, a))$. Furthermore, to address the numerical instability of standard KL-divergence gradients, DSAC decouples the objective into independent mean and standard deviation updates. This separation inversely scales the mean update by variance to reduce step sizes in high-uncertainty regions, thereby curbing overestimation, while stabilizing the variance update via target clipping $C(\cdot; b)$ to prevent optimization collapse

(Duan et al., 2025):

$$\nabla_{\theta} J_Z \approx (\omega + \epsilon_{\omega}) \mathbb{E} \left[\underbrace{- \frac{y_q^{\min} - Q_{\theta}}{\sigma_{\theta}^2 + \epsilon} \nabla_{\theta} Q_{\theta}}_{\text{(I) Mean Update with Expected Value}} - \underbrace{\frac{(C(y_z^{\min}; b) - Q_{\theta})^2 - \sigma_{\theta}^2}{\sigma_{\theta}^3 + \epsilon} \nabla_{\theta} \sigma_{\theta}}_{\text{(II) Variance Update with Clipping}} \right]. \quad (4)$$

Here, y_q^{\min} denotes the conservative target Q-value derived from the twin critics, while y_z^{\min} represents a stochastic sample from the target return distribution. The parameter ϵ is introduced to prevent gradient explosion when the variance σ_{θ}^2 approaches zero, whereas ϵ_{ω} is used to prevent gradient disappearance as the scaling factor ω approaches zero. The scaling factor $\omega = \mathbb{E}_{(s,a) \sim \mathcal{B}}[\sigma_{\theta}(s, a)^2]$ and the clipping boundary b within $C(\cdot; b)$ are adaptively updated based on the running statistics of the learned variance.

As detailed in DSAC-T (Duan et al., 2025), this estimator incorporates three mechanisms: (1) Twin Value Distribution Learning, which mitigates overestimation by computing gradients using the value distribution with the minimum mean Q-value from two independent critics. (2) Expected Value Substituting, which stabilizes mean updates by substituting the stochastic target sample with its analytical expectation in the mean-related gradient term. (3) Variance-Based Critic Gradient Adjustment, which enhances numerical stability and reward robustness by dynamically adjusting the clipping boundary based on variance statistics.

3. Methodology

In this section, we present FastDSAC, a high-throughput reinforcement learning framework tailored for high-dimensional continuous control. FastDSAC adapts the actor-critic paradigm to massive parallelization via structural innovations in both policy parameterization and value estimation. The overall architecture is depicted in Figure 2.

Our method consists of three integrated components: (1) An actor employing Dimension-wise Entropy Modulation (DEM) to autonomously manage exploration budgets in high-dimensional action spaces (Section 3.1); (2) A streamlined Continuous Distributional Critic that enables precise return modeling to eliminate quantization artifacts and mitigate overestimation (Section 3.2); and (3) A unified Distributional Soft Policy Iteration (DSPI) loop optimized for stability in the large-batch regime (Section 3.3).

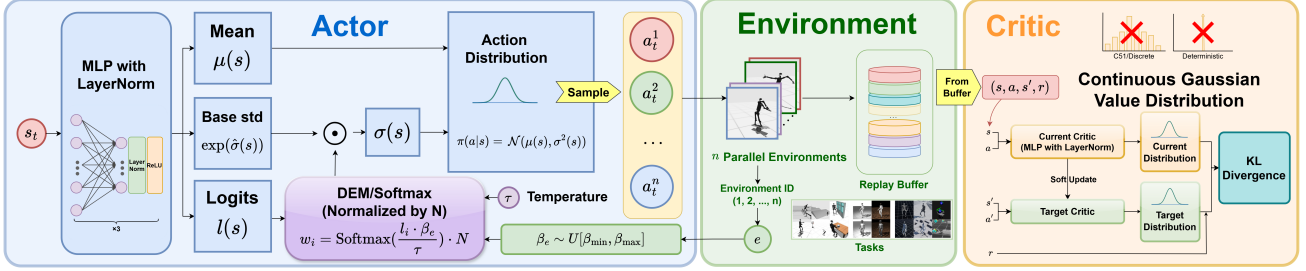


Figure 2. Overview of the FastDSAC architecture. (Left) Actor with DEM: The policy dynamically redistributes the exploration budget by modulating the base standard deviation $\hat{\sigma}(s)$ with weights w_i (via element-wise multiplication \odot). These weights are derived from logits $l(s)$ and an environment-conditioned heterogeneity factor β_e using a normalized Softmax. (Middle) Environment: Massively parallel environments collect uncorrelated experiences into a shared Replay Buffer for high-throughput training. (Right) Continuous Critic: The critic models the value function as a **continuous Gaussian distribution** to mitigate overestimation. It minimizes the **KL Divergence** between the current and target distributions, avoiding the quantization artifacts of discrete baselines (marked by \times).

3.1. The FastDSAC Actor: Dimension-wise Entropy Modulation

Standard Gaussian policies in SAC typically parameterize the action distribution as $\pi_\phi(a|s) = \mathcal{N}(\mu_\phi(s), \text{diag}(\sigma_\phi^2(s)))$, estimating the standard deviation σ_i independently for each dimension. In high-dimensional systems with redundant actuators, this independent parameterization leads to inefficient budget allocation, as the agent squanders exploration variance on task-irrelevant dimensions (Zhang & Cai, 2024; Sferrazza et al., 2024). To address this, we propose Dimension-wise Entropy Modulation (DEM), a mechanism that imposes a structural constraint on the exploration covariance to explicitly manage the variance budget. Rather than replacing the standard variance prediction, our network augments it by predicting a redistribution weight w_i for each dimension $i \in \{1, \dots, |\mathcal{A}|\}$.

Budget-Constrained Variance. Given the actor backbone features $h(s)$, we compute the modulation weights via a temperature-scaled Softmax operation:

$$l_i = f_\phi^{\text{logits}}(h(s))_i, \quad w_i = \frac{\exp(l_i/\tau)}{\sum_{j=1}^N \exp(l_j/\tau)} \cdot N, \quad (5)$$

where τ is a temperature hyperparameter. The factor N (dimension of \mathcal{A}) serves as a normalization constant ensuring that the mean weight is 1 (i.e., $\frac{1}{N} \sum w_i = 1$), effectively enforcing a conservation constraint on the total exploration budget. The final standard deviation for the i -th action dimension is modulated as:

$$\sigma_i(s) = w_i(s) \cdot \exp(\hat{\sigma}_i(s)), \quad (6)$$

where $\hat{\sigma}_i$ represents the base log-scale parameter learned by the network. The subsequent action sampling and policy evaluation follow the standard SAC reparameterization trick.

Interpretation: Autonomous Subspace Pruning. This formulation enforces a soft exploration budget. By dynamically

adjusting w_i , the agent gains the autonomy to selectively suppress noise on specific dimensions while concentrating exploration variance on task-irrelevant dimensions, effectively rendering critical actions near-deterministic to ensure the precise control for optimal convergence. Crucially, this importance assignment is emergent and driven solely by reward maximization. This bypasses the need for manual priors or kinematic specifications, enabling the discovery of effective coordination patterns that may be non-intuitive to human design. As empirically analyzed in Section 4.3, this mechanism effectively prunes the exploration subspace, maintaining high-precision control on stable joints while exploring others. The temperature τ regulates the *sparsity* of this weight distribution: a lower τ encourages a sharp, focused allocation, while a higher τ yields a uniform distribution, approximating standard SAC behavior.

Diversity-driven Population. To mitigate mode collapse across the parallel population, we employ a Heterogeneous Exploration scheme adapted from the work of Seo et al. (2025b). We assign a distinct scaling factor $\beta_e \sim U[\beta_{\min}, \beta_{\max}]$ to each environment e . We assign a distinct scaling factor $\beta_e \sim U[\beta_{\min}, \beta_{\max}]$ to each parallel environment e . Unlike prior works that scale noise magnitude (Li et al., 2023; Seo et al., 2025b), we apply β_e to the modulation logits to vary the distribution shape:

$$w_{i,e} \propto \exp\left(\frac{l_i \cdot \beta_e}{\tau}\right). \quad (7)$$

This effectively diversifies the anisotropy of exploration across the population: some agents explore broadly by distributing the budget across many dimensions, while others focus intensely on specific subspaces, thereby enhancing robustness against local optima.

3.2. The FastDSAC Critic: Streamlined Distributional Learning

To mitigate the quantization errors inherent in discrete critics (Bellemare et al., 2017; Seo et al., 2025b), we adopt the Continuous Gaussian Critic from DSAC-T (Duan et al., 2025), parameterizing the return distribution as $Z_\psi(\cdot|s, a) \sim \mathcal{N}(Q_\psi(s, a), \sigma_\psi^2(s, a))$, to enable precise modeling of the full return distribution.

While the original DSAC-T employs complex variance-based gradient adjustments for low-data regimes, we find these constraints restrict accurate variance modeling in high-throughput settings. Leveraging the natural stability provided by large batch sizes, we streamline the objective by removing variance clipping boundaries, retaining only the core mechanisms of Expected Value Substitution and Gradient Scaling.

The parameters ψ are updated by minimizing the divergence between the predicted distribution and the target. Following the work of Duan et al. (2025), we decompose the gradient into mean-driven and variance-driven components:

$$\nabla_\psi J_Z \approx \omega \cdot \mathbb{E} \left[\underbrace{\left(-\frac{y_q^{\min} - Q_\psi}{\sigma_\psi^2 + \epsilon} \nabla_\psi Q_\psi \right)}_{\text{(I) Stabilized Mean Update}} - \underbrace{\frac{(y_z^{\text{sample}} - Q_\psi)^2 - \sigma_\psi^2}{\sigma_\psi^3 + \epsilon} \nabla_\psi \sigma_\psi}_{\text{(II) Natural Variance Update}} \right]. \quad (8)$$

Here, term (I) leverages the Expected Value Substitution: we anchor the mean update to the conservative target mean $y_q^{\min} = r + \gamma(\min_{j=1,2} Q_{\psi^j}(s', a') - \alpha \log \pi(a'|s'))$, rather than stochastic samples. In high-dimensional context, we find this mechanism is particularly effective at accelerating convergence by filtering out sampling noise inherent in raw stochastic returns. Term (II) updates the variance to capture the intrinsic randomness of the returns. Notably, unlike the original implementation which clips the target sample y_z^{sample} within a dynamic boundary, we remove this constraint to allow the critic to learn the true scale of environmental stochasticity without bias. The scalar $\omega \approx \mathbb{E}_{\mathcal{B}}[\sigma_\psi^2]$ is the gradient scaling factor handling reward scale sensitivity (Duan et al., 2025).

3.3. Distributional Soft Policy Iteration (DSPI)

We integrate the proposed Actor 3.1 and Critic 3.2 into a unified Distributional Soft Policy Iteration (DSPI) loop. This process alternates between evaluating the policy’s return distribution and improving the policy via entropy-regularized maximization. Theoretically, the DSPI framework is guaranteed to converge to the optimal policy, as established in

the work of Duan et al. (2020).

Distributional Soft Policy Evaluation. In the evaluation step, we update the twin critic networks using the streamlined gradient estimator in Eq. (8). By maintaining a continuous Gaussian parameterization, the critic models the full return distribution, explicitly capturing the aleatoric uncertainty alongside the expected return. Crucially, as the gradient magnitude is inversely scaled by this estimated variance, high uncertainty on OOD actions intrinsically dampens updates, serving as a robust regularizer against value overestimation.

Distributional Soft Policy Improvement. In the improvement step, the actor π_ϕ is updated to maximize the expected return and entropy. Following the reparameterization trick (Haarnoja et al., 2018), the actor utilizes the mean estimate of the distributional critic, $Q_\psi(s, a) = \mathbb{E}_{Z \sim Z_\psi}[Z]$, to guide policy updates. The actor loss function to be minimized is:

$$\mathcal{L}_{\text{actor}}(\phi) = \mathbb{E}_{s \sim \mathcal{B}, a \sim \pi_\phi} [\alpha \log \pi_\phi(a|s) - Q_\psi(s, a)]. \quad (9)$$

Since our actor employs the Dimension-wise Entropy Modulation (DEM) mechanism, the term $\log \pi_\phi(a|s)$ implicitly accounts for the redistributed exploration budget. The optimization naturally balances the reward maximization against the structural entropy constraints imposed by DEM, effectively guiding the agent to prune task-irrelevant subspaces. Simultaneously, we automatically tune the temperature parameter α to satisfy a target entropy constraint \mathcal{H} , updating α via gradient descent (Haarnoja et al., 2018):

$$\alpha \leftarrow \alpha - \eta \cdot \mathbb{E}_{s \sim \mathcal{B}, a \sim \pi_\phi} [-\log \pi_\phi(a|s) - \mathcal{H}] \quad (10)$$

Implementation Recipe. To ensure stability and peak performance in the high-throughput regime, we adopt specific engineering choices grounded in recent literature:

- **Layer Normalization (LayerNorm):** We apply LayerNorm in the actor and critic networks specifically for the ultra-high-dimensional HumanoidBench domain ($|\mathcal{A}| = 61$), improving training stability and final performance. Consistent with recent findings (Ball et al., 2023; Nauman et al., 2024; Seo et al., 2025a), this regularization proves critical for stability in such expansive spaces. Conversely, for the lower-dimensional MuJoCo Playground and IsaacLab tasks, FastDSAC achieves SOTA performance without LayerNorm, demonstrating that our method’s superiority stems from its core mechanism rather than architectural dependencies.
- **Target Entropy:** Following recent work (Seo et al., 2025a), we set the target entropy $\mathcal{H} = 0$ across all tasks. In high-dimensional spaces, the standard heuristic $\mathcal{H} = -\dim(\mathcal{A})$ prescribes a highly negative entropy target, which often forces the policy into a low-variance regime prematurely, exacerbating the “vanishing exploration” problem. By raising the target to

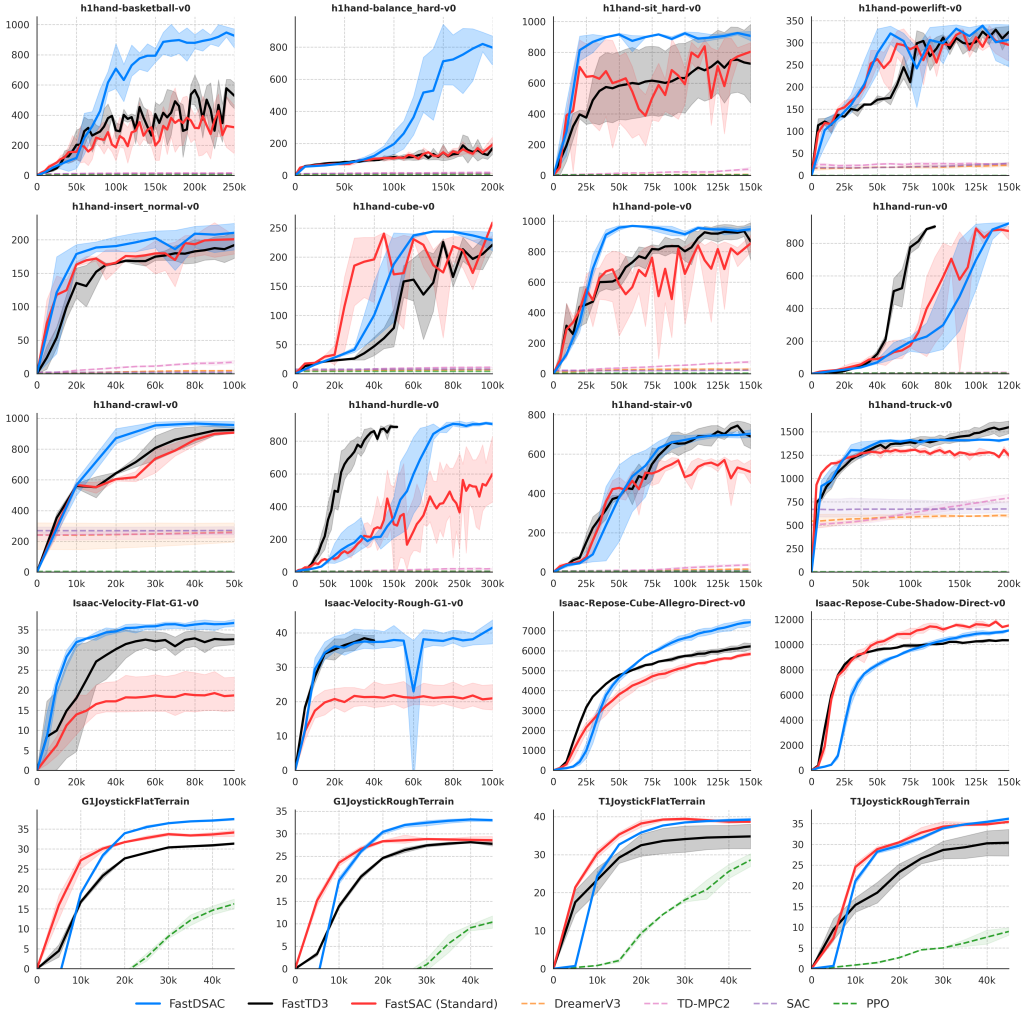


Figure 3. Comparative evaluation on high-dimensional continuous control benchmarks. Learning curves across selected tasks from HumanoidBench (top two rows), IsaacLab (third row), and MuJoCo Playground (bottom row). FastDSAC consistently matches or outperforms FastTD3 and FastSAC (Standard). Notably, FastDSAC excels in precision-demanding (e.g., Basketball, Insert) and stability-critical (e.g., Balance Hard) tasks, while maintaining robust dexterous manipulation and rough-terrain locomotion performance.

$\mathcal{H} = 0$, we explicitly maintain a substantial exploration budget to prevent premature convergence. Crucially, while this increased budget implies higher aggregate randomness, our DEM mechanism acts as a structural filter, channeling this exploration budget primarily into task-relevant dimensions while effectively suppressing noise on redundant actuators.

- **High-Precision Critic Stability:** Unlike the original DSAC-T which requires a large numerical stabilizer (bias = 0.1) to prevent division-by-zero, the stable statistics from our large batch sizes allow us to reduce this bias to 10^{-6} . This enables the FastDSAC critic to model low-variance states with significantly higher fidelity, capturing fine-grained reward structures that are otherwise smoothed out by conservative stabilization.

4. Experiments

Our evaluation validates the scalability of FastDSAC in high-dimensional continuous control, addressing four key questions: **Q1 (Comparative Performance):** Can FastDSAC outperform SOTA deterministic (FastTD3), Standard stochastic (FastSAC), on-policy (PPO, (Schulman et al., 2017)), and model-based (e.g., DreamerV3) baselines across complex domains? **Q2 (Actor Ablation):** Is Dimension-wise Entropy Modulation (DEM) necessary, and does it yield interpretable, task-aligned structures? **Q3 (Critic Ablation):** Does Continuous Gaussian modeling offer superior stability over discrete C51 approximations? **Q4 (Structural Sensitivity):** How does τ regulate the sparsity of the exploration budget?

To address these, we evaluated our method on Humanoid-

Bench, MuJoCo Playground, and IsaacLab, spanning tasks from locomotion to complex whole-body manipulation.

4.1. Experimental Setup

Benchmarks. We aligned with the FastTD3 suite (Seo et al., 2025b), evaluating on: (1) HumanoidBench (Sferazza et al., 2024): 29 representative tasks spanning locomotion and whole-body manipulation, characterized by high-dimensional action spaces ($|\mathcal{A}| = 61$). (2) MuJoCo Playground (Zakka et al., 2025) & IsaacLab (Mittal et al., 2023): 10 tasks across diverse physics engines to verify robustness. Given the moderate dimensionality ($|\mathcal{A}| < 30$) compared to HumanoidBench, we omitted Layer Normalization, as FastDSAC retains inherent stability without it.

Baselines & Protocol. We benchmarked against FastTD3 (deterministic SOTA) and FastSAC (parallelized stochastic baseline) (Seo et al., 2025b). To ensure rigorous comparison in high dimensions, we enhanced the standard FastSAC with Layer Normalization and target entropy $\mathcal{H} = 0$, hereafter denoted as *FastSAC (standard)*. For HumanoidBench, we additionally compared against DreamerV3, TD-MPC2, SAC, and PPO using official benchmarks; for MuJoCo Playground and IsaacLab, we additionally evaluated against PPO to contextualize performance against on-policy method in these domains. We report mean returns aggregated over 3 seeds, with shaded regions indicating the min-max range. Hyperparameters are detailed in Appendix A.

4.2. Main Results

We evaluated FastDSAC across 39 tasks spanning diverse dynamics. Figure 3 illustrates learning curves for 20 representative tasks from HumanoidBench, MuJoCo Playground, and IsaacLab (see Appendix E for full results). Our analysis reveals three distinct performance regimes:

Dominance in Complex Coordination & Manipulation. FastDSAC establishes a new SOTA on tasks demanding precise actuation and whole-body coordination, significantly outperforming FastTD3 and FastSAC (Standard) baselines on challenging tasks such as *Basketball*, *Balance Hard*, *Insert Normal*, *Sit Hard*, and *Pole*. This gap highlights the limitation of deterministic policies in exploring intricate control manifolds, whereas FastDSAC’s entropy modulation effectively prunes the action space to discover superior solutions otherwise inaccessible to standard methods.

The Exploration-Exploitation Trade-off in Locomotion. In dynamic locomotion (e.g., *Run*, *Hurdle*), we observe a distinct learning profile: FastDSAC exhibits a slower initial rise compared to the aggressive exploitation of FastTD3, yet converges to a higher final return. This behavior aligns with the maximum entropy objective, where DEM initially invests budget in exploring diverse gait patterns before sta-

bilizing, whereas FastTD3 often converges prematurely to suboptimal gaits. Even on complex whole-body control tasks like *Truck* and *Stair*, FastDSAC remains competitive with FastTD3. This demonstrates that our framework effectively constrains the variance inherent to stochastic policies, retaining the necessary control authority for rigorous terrain adaptation and long-horizon object manipulation.

Robustness Across Simulators. FastDSAC scales consistently across diverse physics engines. In MuJoCo Playground (e.g., *G1/T1 Joystick*), it maintains a clear lead. In IsaacLab (*Velocity-Rough*, *Repose-Cube-Allegro/Shadow*), FastDSAC surpasses FastTD3 after an initial adaptation phase, validating its robustness across dynamics. While *Repose-Cube-Shadow* presents a unique outlier where FastSAC (Standard) leads—suggesting that for specific lower-dimensional hand-only tasks ($|\mathcal{A}| \approx 24$), raw stochasticity may suffice—FastDSAC remains the superior generalist across the broader benchmark suite.

4.3. Ablation Studies and Analysis

To dissect component necessity, we conducted ablation studies on representative tasks spanning three core challenges: precision contact (*Basketball*), limit-handling stability (*Balance Hard*), and dynamic locomotion (*Hurdle* or *Stair*).

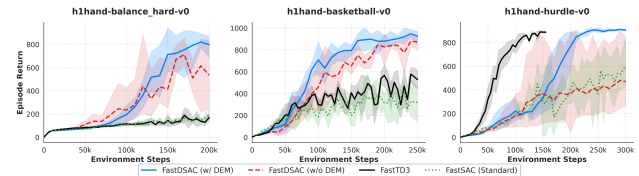


Figure 4. Ablation study of DEM. Learning curves on HumanoidBench tasks (*Balance Hard*, *Basketball*, *Hurdle*) comparing FastDSAC (w/ vs. w/o DEM) against FastTD3 and FastSAC baselines.

Q2: Necessity and Mechanism of Dimension-wise Entropy Modulation (DEM). To evaluate DEM, we compared FastDSAC against a variant (w/o DEM) that substitutes the entropy-modulated actor with a standard diagonal Gaussian policy. Figure 4 shows that removing DEM consistently degrades performance. In *Balance Hard* and *Basketball*, while the ablated agent still outperforms baselines (due to the continuous gaussian critic), it significantly lags behind FastDSAC. Crucially, FastDSAC (w/o DEM) exhibits high inter-seed variance in the *Hurdle* task, indicating that omitting DEM hampers the management of high-dimensional exploration and leads to seed-sensitive policies.

Visualizing the Mechanism: Autonomous Subspace Pruning. To understand how DEM optimizes exploration, we analyzed the evolution of learned weights w_i and corresponding robot behaviors during a *Basketball* episode (Figure 5; see heatmap Figure 8 in Appendix D). The visual-

ization reveals a task-aligned exploration allocation strategy governed by the conservation constraint of the Softmax normalization ($\frac{1}{N} \sum w_i = 1$). This enforces a zero-sum game: to reduce variance on critical joints, the agent must increase variance elsewhere. **1) Variance Concentration:** We observed a prominent high-weight band (bright yellow) corresponding to the left hand thumb joints (e.g., `lh_A_THJ4`) and wrist, which reach values as high as $w_i \approx 8.0$. **2) Precision for Impact and Balance:** During the critical interaction phase (Steps 10-13), as the robot impacts the ball towards the hoop, weights for the legs, torso, and right arm are suppressed to near-zero. This suppression persists post-impact to counteract momentum and maintain balance, contrasting with the high-variance thumb.

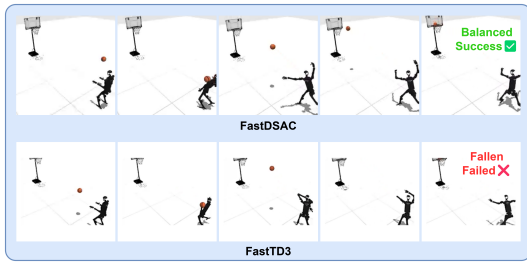


Figure 5. **Qualitative comparison on Basketball.** FastDSAC (Top) coordinates the throw successfully while maintaining stability, whereas FastTD3 (Bottom) loses balance and fails.

Interpretation: Emergent Strategy via Variance Offloading. The agent autonomously discovers an unconventional “body-rebound” strategy, utilizing the torso rather than hands to redirect the ball. While counter-intuitive to human design, this behavior maximizes the total return by prioritizing post-throw stability over risky dexterity. The heatmap confirms that the agent treats the task-irrelevant left thumb as an *entropy sink* for the required exploration budget. By offloading variance to these distal joints, FastDSAC effectively prunes the exploration subspace, preserving high-precision control for the core body and legs to attain consistent returns of ≈ 1032 . Crucially, despite kinematic variations across seeds, the variance redistribution structure remains invariant: FastDSAC consistently exploits task-irrelevant subspaces as entropy sinks to stabilize control.

Contrast with Deterministic Baseline. FastTD3 attempts an intuitive but unstable hand-catch strategy, as depicted in Figure 5. However, it fails to balance manipulation with whole-body stability, hitting the ball but subsequently falling (return ≈ 500). This highlights a critical advantage: unlike deterministic policies prone to unstable local optima, FastDSAC’s entropy modulation uncovers robust, global-optimum behaviors, even those that expose the subtleties of high-dimensional reward specification.

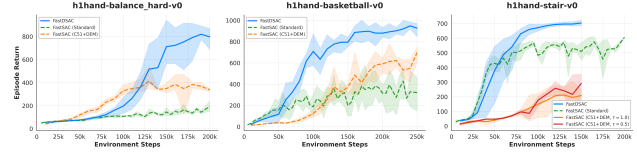


Figure 6. **Comparison of continuous and discrete value estimation.** Evaluation on high-dimensional humanoid tasks. Curves show the mean episode return of FastDSAC compared to FastSAC (C51+DEM) and FastSAC (standard).

Q3: Continuous vs. Discrete Distributional Critics. To isolate the impact of our continuous critic, we compared FastDSAC against a discrete baseline: the C51-variant of FastSAC (Seo et al., 2025a) augmented with our DEM module. Hyperparameters are held constant to strictly isolate the efficacy of the continuous parameterization. Figure 6 shows FastDSAC consistently outperforms both FastSAC (standard) and its discrete variant (FastSAC with C51+DEM), notably achieving $\approx 2\times$ higher returns in *Balance Hard*. This gap highlights the precision limits of discrete atoms, where inevitable quantization errors compromise value fidelity. In contrast, FastDSAC’s continuous Gaussian parameterization eliminates these artifacts, enabling the precise value modeling required for superior control.

4.4. Sensitivity Analysis

Q4: Impact of Temperature τ . τ governs the exploration weight distribution across action dimensions. Higher τ promotes uniform allocation, whereas lower τ induces a “winner-takes-all” effect, concentrating weights on specific dimensions (visualized across varying temperatures in Appendix D, Figure 9).

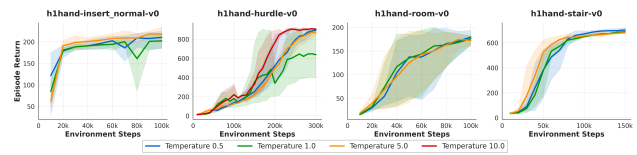


Figure 7. **Sensitivity analysis of the DEM temperature.** FastDSAC is evaluated on four HumanoidBench tasks (*Insert Normal, Hurdle, Room, Stair*) under varying $\tau \in \{0.5, 1.0, 5.0, 10.0\}$.

Figure 7 reveals that the optimal τ depends on specific task dynamics. Notably, *Hurdle* achieves peak performance at a high temperature ($\tau = 10.0$), where a uniform allocation prevents premature subspace collapse, preserving the structural diversity essential for coordinated gaits. Conversely, while most tasks are robust to a default setting, tailoring τ allows for further performance optimization by aligning with the distinct exploration granularity of specific dynamics.

5. Conclusion

We challenge the dominance of deterministic policy gradients in high-dimensional control with FastDSAC, a framework that unlocks the scalability of maximum entropy RL. By integrating Dimension-wise Entropy Modulation (DEM) for autonomous subspace pruning and a continuous distributional critic to ensure value fidelity and curb overestimation, we effectively overcome the “curse of dimensionality.” Across 39 diverse tasks, FastDSAC consistently matches or outperforms SOTA baselines, achieving remarkable gains of 180% and 400% on complex coordination tasks. Our findings demonstrate that rigorously designed stochastic policies are not merely viable but superior for high-throughput robotics, bridging the gap between broad exploration and high-precision control. Future work will investigate leveraging DEM’s emergent structures to automatically discover low-dimensional motor primitives for hierarchical planning.

Impact Statement

By facilitating the efficient acquisition of complex, dynamic behaviors in high-dimensional humanoid control, our framework has the potential to advance general-purpose robotics. These capabilities are particularly relevant for deploying robots in unstructured, critical environments, such as search and rescue, industrial automation, and assistive healthcare, thereby democratizing access to sophisticated motor skills without prohibitive computational costs. However, the deployment of such agile autonomous systems raises valid safety concerns regarding unintended physical interaction and potential long-term economic impacts on the workforce. Consequently, real-world application of these policies necessitates robust verification protocols and rigorous safety constraints to prevent accidents and ensure physical safety.

References

- Ball, P. J., Smith, L., Kostrikov, I., and Levine, S. Efficient online reinforcement learning with offline data. In *International Conference on Machine Learning*, 2023.
- Bellemare, M. G., Dabney, W., and Munos, R. A distributional perspective on reinforcement learning, 2017. URL <https://arxiv.org/abs/1707.06887>.
- Bhatt, A., Argus, M., Amiranashvili, A., and Brox, T. Crossq: Batch normalization in deep reinforcement learning for greater sample efficiency and simplicity. *ArXiv*, abs/1902.05605, 2019.
- Duan, J., Guan, Y., Li, S., Ren, Y., Sun, Q., and Cheng, B. Distributional soft actor-critic: Off-policy reinforcement learning for addressing value estimation errors. *IEEE Transactions on Neural Networks and Learning Systems*, 33:6584–6598, 2020.
- Duan, J., Wang, W., Xiao, L., Gao, J., Li, S. E., Liu, C., Zhang, Y.-Q., Cheng, B., and Li, K. Distributional soft actor-critic with three refinements. *IEEE Transactions on Pattern Analysis and Machine Intelligence*, 47(5):3935–3946, 2025. doi: 10.1109/TPAMI.2025.3537087.
- Fujimoto, S., Hoof, H., and Meger, D. Addressing function approximation error in actor-critic methods. In *International Conference on Machine Learning*, 2018.
- Gallici, M., Fellows, M., Ellis, B., Pou, B., Masmitja, I., Foerster, J. N., and Martin, M. Simplifying deep temporal difference learning. In *The Thirteenth International Conference on Learning Representations*, 2025. URL <https://openreview.net/forum?id=7IzeL0kflu>.
- Haarnoja, T., Zhou, A., Abbeel, P., and Levine, S. Soft actor-critic: Off-policy maximum entropy deep reinforcement learning with a stochastic actor. In *International conference on machine learning*, pp. 1861–1870. Pmlr, 2018.
- Hafner, D., Pasukonis, J., Ba, J., and Lillicrap, T. Mastering diverse domains through world models. *arXiv preprint arXiv:2301.04104*, 2023.
- Hansen, N., Su, H., and Wang, X. Td-mpc2: Scalable, robust world models for continuous control. In *International Conference on Learning Representations*, 2024.
- Kaufmann, E., Bauersfeld, L., Loquercio, A., Müller, M., Koltun, V., and Scaramuzza, D. Champion-level drone racing using deep reinforcement learning. *Nature*, 620 (7976):982–987, 2023.
- Köppen, M. The curse of dimensionality. In *5th Online World Conference on Soft Computing in Industrial Applications (WSC5)*, volume 1, pp. 4–8, 2000.
- Kuznetsov, A., Shvechikov, P., Grishin, A., and Vetrov, D. Controlling overestimation bias with truncated mixture of continuous distributional quantile critics, 2020. URL <https://arxiv.org/abs/2005.04269>.
- Li, Z., Chen, T., Hong, Z.-W., Ajay, A., and Agrawal, P. Parallel q -learning: Scaling off-policy reinforcement learning under massively parallel simulation. In *International Conference on Machine Learning*, pp. 19440–19459. PMLR, 2023.
- Loshchilov, I. and Hutter, F. Decoupled weight decay regularization. *arXiv preprint arXiv:1711.05101*, 2017.
- Mittal, M., Yu, C., Yu, Q., Liu, J., Rudin, N., Hoeller, D., Yuan, J. L., Singh, R., Guo, Y., Mazhar, H., Mandlekar, A., Babich, B., State, G., Hutter, M., and Garg,

- A. Orbit: A unified simulation framework for interactive robot learning environments. *IEEE Robotics and Automation Letters*, 8(6):3740–3747, 2023. doi: 10.1109/LRA.2023.3270034.
- Nauman, M., Ostaszewski, M., Jankowski, K., Miłoś, P., and Cygan, M. Bigger, regularized, optimistic: scaling for compute and sample-efficient continuous control. In *Advances in Neural Information Processing Systems*, 2024.
- Neumann, G., Otto, F., Becker, P., and Vien, N. A. Vlearn: Off-policy learning with efficient state-value function estimation, 2024. URL <https://arxiv.org/abs/2403.04453>.
- Obando-Ceron, J., Mayor, W., Lavoie, S., Fujimoto, S., Courville, A., and Castro, P. S. Simplicial embeddings improve sample efficiency in actor-critic agents, 2025. URL <https://arxiv.org/abs/2510.13704>.
- Rudin, N., Hoeller, D., Reist, P., and Hutter, M. Learning to walk in minutes using massively parallel deep reinforcement learning. In *Proceedings of the 5th Conference on Robot Learning*, volume 164 of *Proceedings of Machine Learning Research*, pp. 91–100. PMLR, 2022. URL <https://proceedings.mlr.press/v164/rudin22a.html>.
- Schulman, J., Wolski, F., Dhariwal, P., Radford, A., and Klimov, O. Proximal policy optimization algorithms. *arXiv preprint arXiv:1707.06347*, 2017.
- Schumacher, P., Geijtenbeek, T., Caggiano, V., Kumar, V., Schmitt, S., Martius, G., and Haeufle, D. F. B. Natural and robust walking using reinforcement learning without demonstrations in high-dimensional musculoskeletal models, 2023. URL <https://arxiv.org/abs/2309.02976>.
- Seo, Y. and Abbeel, P. Coarse-to-fine q-network with action sequence for data-efficient reinforcement learning, 2025. URL <https://arxiv.org/abs/2411.12155>.
- Seo, Y., Sferrazza, C., Chen, J., Shi, G., Duan, R., and Abbeel, P. Learning sim-to-real humanoid locomotion in 15 minutes, 2025a. URL <https://arxiv.org/abs/2512.01996>.
- Seo, Y., Sferrazza, C., Geng, H., Nauman, M., Yin, Z.-H., and Abbeel, P. Fasttd3: Simple, fast, and capable reinforcement learning for humanoid control. *arXiv preprint arXiv:2505.22642*, 2025b.
- Sferrazza, C., Huang, D.-M., Lin, X., Lee, Y., and Abbeel, P. Humanoidbench: Simulated humanoid benchmark for whole-body locomotion and manipulation. In *Robotics: Science and Systems*, 2024.
- Shukla, A. Speeding up sac with massively parallel simulation. <https://arthshukla.substack.com>, Mar 2025. URL <https://arthshukla.substack.com/p/speeding-up-sac-with-massively-parallel>.
- Wei, Y., Zuo, C., and Sui, Y. Scalable exploration for high-dimensional continuous control via value-guided flow, 2026. URL <https://arxiv.org/abs/2601.19707>.
- Zakka, K., Tabanpour, B., Liao, Q., Haiderbhai, M., Holt, S., Luo, J. Y., Allshire, A., Frey, E., Sreenath, K., Kahrs, L. A., et al. Mujoco playground. *arXiv preprint arXiv:2502.08844*, 2025.
- Zhang, W. and Cai, H. On high-dimensional action selection for deep reinforcement learning, 2024. URL <https://openreview.net/forum?id=rto6aU453A>.
- Zhuang, Z., Shi, D., Suo, R., He, X., Zhang, H., Wang, T., Lyu, S., and Wang, D. Tdmpbc: Self-imitative reinforcement learning for humanoid robot control. *arXiv preprint arXiv:2502.17322*, 2025.

A. Hyperparameters

Table 1. FastDSAC Hyperparameter specifications. The following parameters are kept constant across all tasks: Actor/Critic/Alpha LR = 3×10^{-4} , Batch Size = 32,768, $\tau = \tau_b = 0.005$, Weight Decay = 1×10^{-4} , Learning Starts = 1000, Target Entropy Ratio = 0, Log Std Min = -10, Scale Max (β_{\max}) = 2, and Activation = ReLU. We distinguish defaults by domain: HumanoidBench tasks utilize Alpha Init = 0.001 and enable Layer Normalization, whereas IsaacLab and MuJoCo Playground tasks use Alpha Init = 0.01 and do not utilize Layer Normalization.

Environment	Gamma	Buffer Size	Log Std Max	Scale Min (β_{\min})	Temperature	Total Timesteps
HumanoidBench						
h1hand_slide_v0	0.99	51200	0.5	0.01	0.5	200000
h1hand_stand_v0	0.99	51200	0.5	0.01	1	50000
h1hand_run_v0	0.99	51200	0.5	0.01	1	200000
h1hand_package_v0	0.99	51200	0.5	0.01	1	100000
h1hand_truck_v0	0.99	51200	0.5	0.01	1	200000
h1hand_walk_v0	0.99	51200	0.5	0.01	0.5	100000
h1hand_sit_hard_v0	0.99	51200	0.5	0.01	1	150000
h1hand_pole_v0	0.99	51200	0.5	0.01	1	150000
h1hand_window_v0	0.99	51200	0.5	0.01	1	250000
h1hand_powerlift_v0	0.99	51200	1	0.01	1	150000
h1hand_sit_simple_v0	0.99	51200	0.5	0.01	1	100000
h1hand_bookshelf_hard_v0	0.99	51200	0.5	0.01	1	150000
h1hand_maze_v0	0.99	51200	0.5	0.01	1	100000
h1hand_basketball_v0	0.99	51200	0.5	0.01	0.5/1	250000
h1hand_insert_small_v0	0.99	51200	0.5	0.01	1	100000
h1hand_reach_v0	0.99	51200	1	0.01	1	200000
h1hand_insert_normal_v0	0.99	51200	0.5	0.01	0.5	100000
h1hand_balance_hard_v0	0.99	51200	1	0.01	1	200000
h1hand_crawl_v0	0.99	51200	0.5	0.01	1	60000
h1hand_spoon_v0	0.99	51200	0.5	0.01	1	200000
h1hand_stair_v0	0.99	51200	1	0.1	0.5	150000
h1hand_bookshelf_simple_v0	0.99	51200	0.5	0.01	1	100000
h1hand_balance_simple_v0	0.99	51200	1	0.01	1	200000
h1hand_cabinet_v0	0.99	51200	1	0.01	1	100000
h1hand_door_v0	0.99	51200	0.5	0.01	1	100000
h1hand_cube_v0	0.99	51200	0.5	0.01	1	100000
h1hand_push_v0	0.99	51200	1	0.01	1	500000
h1hand_room_v0	0.99	51200	1	0.01	5	100000
h1hand_hurdle_v0	0.99	51200	1	0.01	10	300000
IsaacLab						
Isaac_Velocity_Rough_G1_v0	0.99	5120	1	0.01	1	100000
Isaac_Velocity_Flat_G1_v0	0.99	10240	1	0.01	1	100000
Isaac_Repose_Cube_Shadow_Direct_v0	0.99	10240	1	0.01	1	200000
Isaac_Repose_Cube_Allegro_Direct_v0	0.99	10240	1	0.01	1	200000
Isaac_Velocity_Rough_H1_v0	0.99	5120	1	0.01	1	100000
Isaac_Velocity_Flat_H1_v0	0.99	10240	1	0.01	1	100000
Mujoco Playground						
T1JoystickRoughTerrain	0.97	10240	1	0.01	1	100000
T1JoystickFlatTerrain	0.97	10240	1	0.01	1	100000
G1JoystickRoughTerrain	0.97	10240	1	0.01	1	100000
G1JoystickFlatTerrain	0.97	10240	1	0.01	1	100000

Our experimental setup is largely adopted from FastTD3 (Seo et al., 2025b), particularly regarding *Buffer Size* and *Total Timesteps*. Empirically, the algorithm requires minimal tuning for most tasks, while performance is sensitive to *Log_Std_Max*, *alpha_init*, and *temperature* in certain tasks.

For the optimization process, we utilize the AdamW optimizer (Loshchilov & Hutter, 2017), following the configuration in the work of Seo et al. (2025a). Specifically, we use fused kernels for efficiency and set the momentum parameters to $\beta = (0.9, 0.95)$ to improve stability in high-dimensional spaces. Detailed hyperparameters of FastDSAC are listed in Table 1.

Baseline Configurations. To ensure rigorous evaluation, results for the FastTD3 baseline are sourced directly from the work of Seo et al. (2025b), ensuring comparison against the fully optimized SOTA deterministic method. For the FastSAC baseline, we adopt the standard hyperparameter configuration: log-standard deviation bounds $[-5, 2]$, discount factor $\gamma = 0.99$, weight decay 0.1, and soft update rate $\tau = 0.1$. However, to provide a competitive maximum entropy baseline in high-dimensional domains, we equip the FastSAC architecture with Layer Normalization and set the target entropy $\mathcal{H} = 0$. This ensures it benefits from the same regularization stability and exploration scale as our proposed method.

B. Related Work

Scalable Reinforcement Learning for High-Dimensional Control. Recent advances in physics simulation have shifted the paradigm of RL-based high-dimensional humanoid control towards massive parallelism (Rudin et al., 2022; Mittal et al., 2023; Zakka et al., 2025). In this high-throughput regime, deterministic policy gradient methods, exemplified by FastTD3 (Seo et al., 2025b) and Parallel Q-Learning (PQL) (Li et al., 2023), have established themselves as the dominant approach due to their perceived training stability in expansive action spaces. While model-based approaches like DreamerV3 (Hafner et al., 2023), TD-MPC2 (Hansen et al., 2024), and TDMPBC (Zhuang et al., 2025) offer strong sample efficiency, they often incur prohibitive computational overhead for world model inference, negating the wall-clock speedup benefits of parallel simulation. Theoretically, Maximum Entropy RL (e.g., SAC) offers superior exploration and robustness properties (Haarnoja et al., 2018). However, its application to high-dimensional domains ($|\mathcal{A}| > 60$) has been impeded by the "curse of dimensionality," often necessitating substantial architectural modifications or yielding inferior performance compared to deterministic baselines (Obando-Ceron et al., 2025; Seo et al., 2025b). FastDSAC challenges this compromise. By introducing Dimension-wise Entropy Modulation (DEM) to impose structural constraints on the exploration covariance, we demonstrate that a rigorously designed stochastic policy can be revitalized to achieve superior control efficacy, outperforming deterministic baselines by significant margins while retaining the exploration benefits essential for complex coordination.

Maximum Entropy RL and Value Estimation in High Dimensions. Scaling Soft Actor-Critic to high-dimensional spaces introduces two fundamental pathologies: inefficient exploration and value overestimation. First, standard Gaussian policies suffer from "vanishing exploration" (Wei et al., 2026), where exploration volume collapses in high dimensions, leading to inefficient variance allocation on task-irrelevant actuators (Zhang & Cai, 2024). While prior works like QFLEX (Wei et al., 2026) attempt to mitigate this via heavy flow-based generative models, our DEM mechanism offers a lightweight, structure-aware solution that autonomously prunes the exploration subspace without additional inference latency. Second, maintaining accurate Q-functions in high-dimensional spaces is notoriously difficult due to "Q-bias explosion" on OOD actions (Bhatt et al., 2019; Neumann et al., 2024). Although TQC (Kuznetsov et al., 2020) and FastTD3 (Seo et al., 2025b) employ distributional RL with truncated quantiles or categorical atoms (C51) to dampen these biases, their discrete nature introduces quantization errors. Crucially, we find these errors catastrophic for precision-demanding humanoid tasks (e.g., basketball, insertion), where fine-grained signal propagation is paramount. In contrast, FastDSAC leverages a Continuous Gaussian Critic (Duan et al., 2025). Distinct from the original DSAC-T formulation, we streamline the variance objective by removing restrictive clipping boundaries to accommodate the high-variance dynamics of massive parallelism. This enables infinite-precision modeling of the return distribution, effectively eliminating quantization artifacts while robustly mitigating overestimation via uncertainty-aware gradient scaling.

C. Computational Resources

We conducted our experiments on a heterogeneous computing cluster consisting of high-performance workstations. The experiments were distributed across two primary hardware configurations:

- **Configuration A:** Equipped with an Intel Core i7-14700K CPU (20 physical cores, 28 logical threads) and 128 GB of

system RAM. Accelerated computing was provided by a single NVIDIA GeForce RTX 4090.

- **Configuration B:** Equipped with an AMD Ryzen 9 9950X CPU (16 physical cores, 32 logical threads) and 192 GB of system RAM. This node features an NVIDIA RTX 6000 (Blackwell Workstation Edition) with 96 GB of VRAM, facilitating large-scale parallel training.

Resource Allocation. To ensure efficient training and accommodate varying memory requirements, tasks were assigned to specific configurations. The memory-intensive IsaacLab environments—specifically *Isaac-Velocity-Flat-G1-v0*, *Isaac-Velocity-Rough-G1-v0*, *Isaac-Repose-Cube-Allegro-Direct-v0*, and *Isaac-Repose-Cube-Shadow-Direct-v0*—were trained on **Configuration B** to leverage its extensive VRAM capacity. All other tasks, including the HumanoidBench and MuJoCo Playground suites, were trained on **Configuration A**. This hardware setup ensured efficient training on high-dimensional tasks, with each experiment converging in under 8 hours.

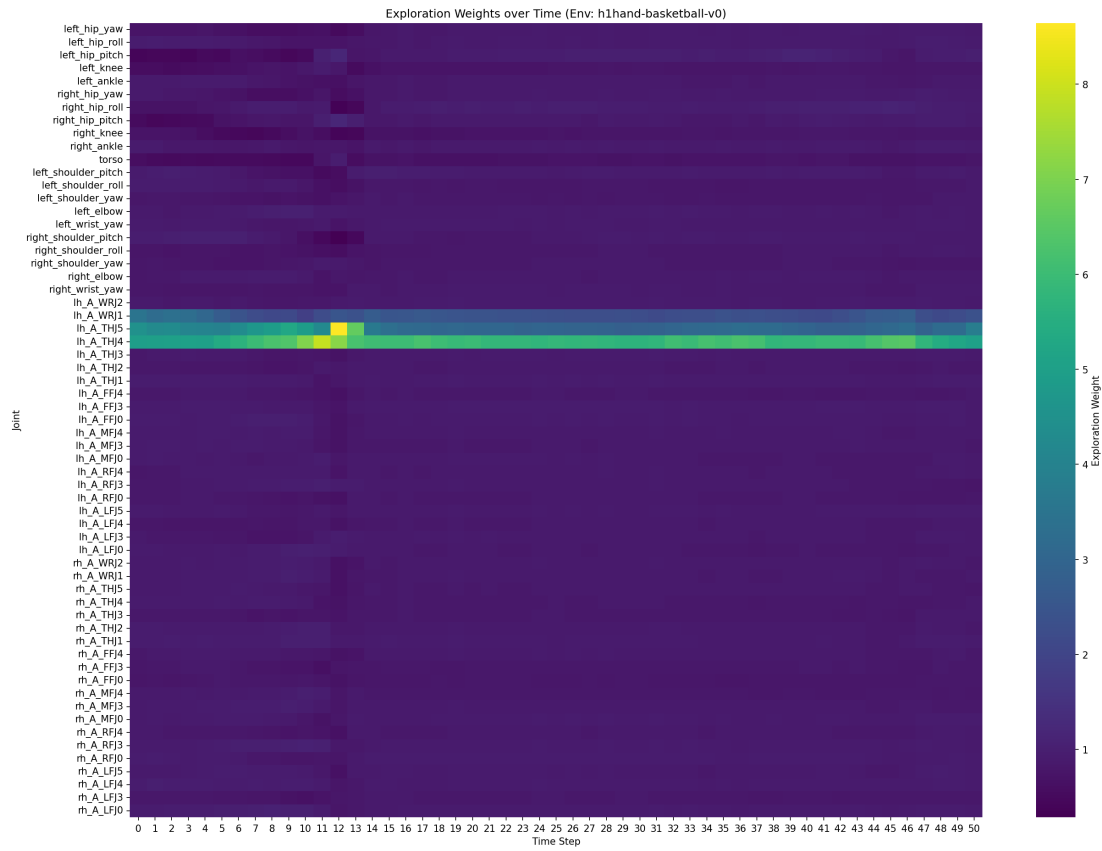
D. Heatmaps of *Basketball* Task

Figure 8. Exploration weights (w_i) during a Basketball episode. High weights (bright) concentrate on the left thumb and wrist, while lower weights (dark) on the legs, torso, and right arm.

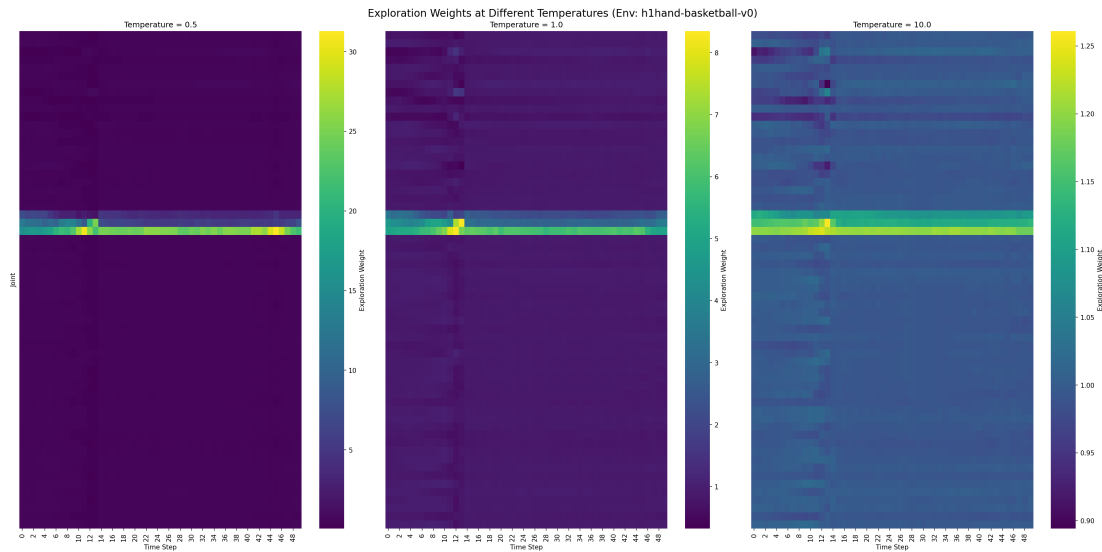


Figure 9. Visualization of exploration weights at different temperatures. Lower temperatures ($\tau = 0.5$) result in highly concentrated weights on specific active joints, whereas higher temperatures ($\tau = 10.0$) lead to a nearly uniform distribution across all joints.

E. Full Results

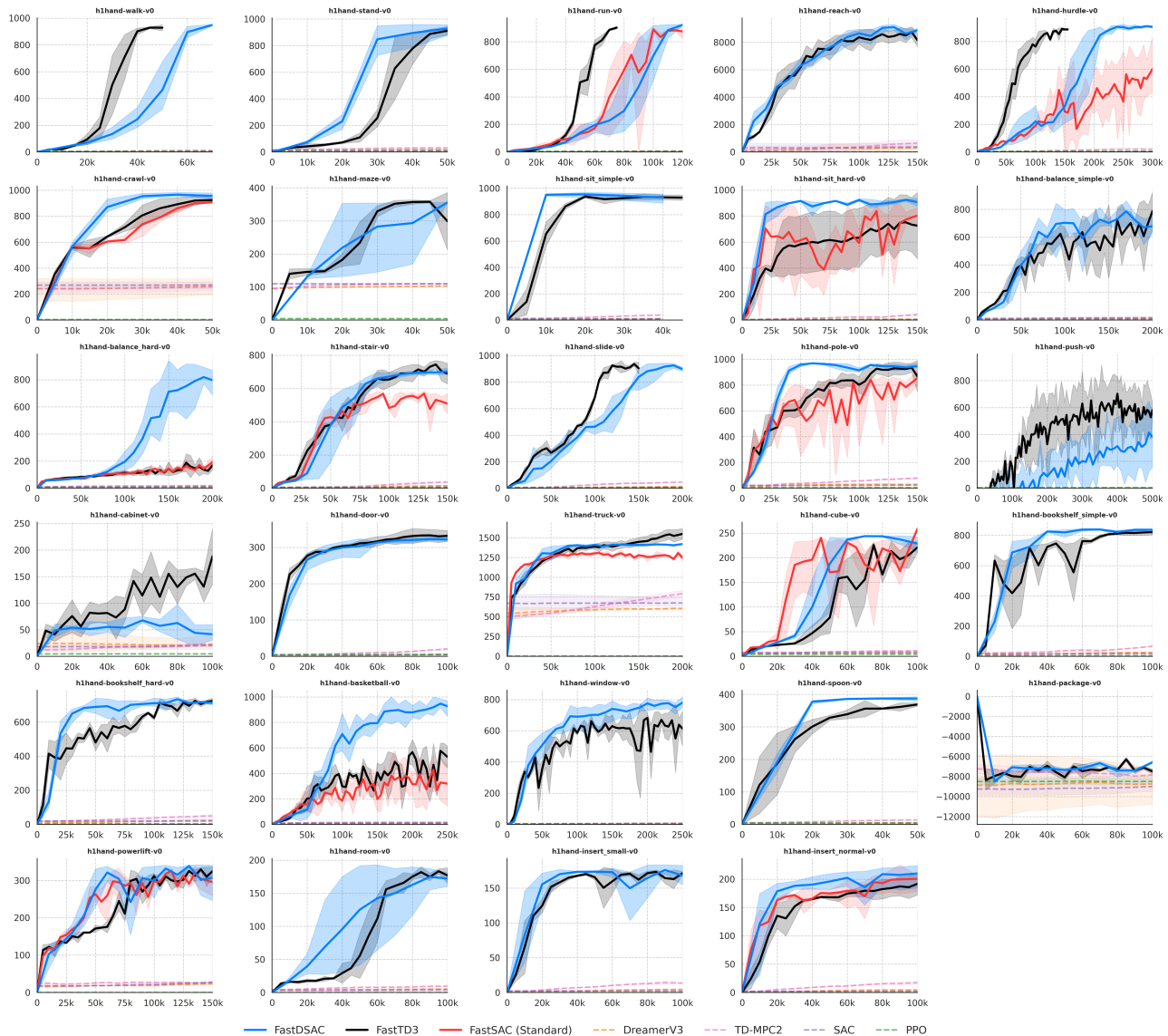


Figure 10. Full Results on HumanoidBench (29 Tasks). We evaluate FastDSAC (blue) against deterministic FastTD3 (black), stochastic FastSAC (Standard) (red), and leading baselines including DreamerV3 (orange), TD-MPC2 (pink), SAC (purple), and PPO (green). Curves depict the mean return over training steps, with shaded regions indicating the min-max range across 3 seeds. FastDSAC consistently achieves state-of-the-art sample efficiency across a broad spectrum of high-dimensional control tasks, ranging from locomotion (e.g., Run, Hurdle) to fine manipulation (e.g., Insert) and complex whole-body coordination (e.g., Basketball, Balance). Notably, FastDSAC demonstrates superior exploration capabilities compared to deterministic baselines while maintaining higher stability and asymptotic performance than standard stochastic counterparts. **Note: For FastSAC (Standard), we report results on a subset of 12 representative tasks.**

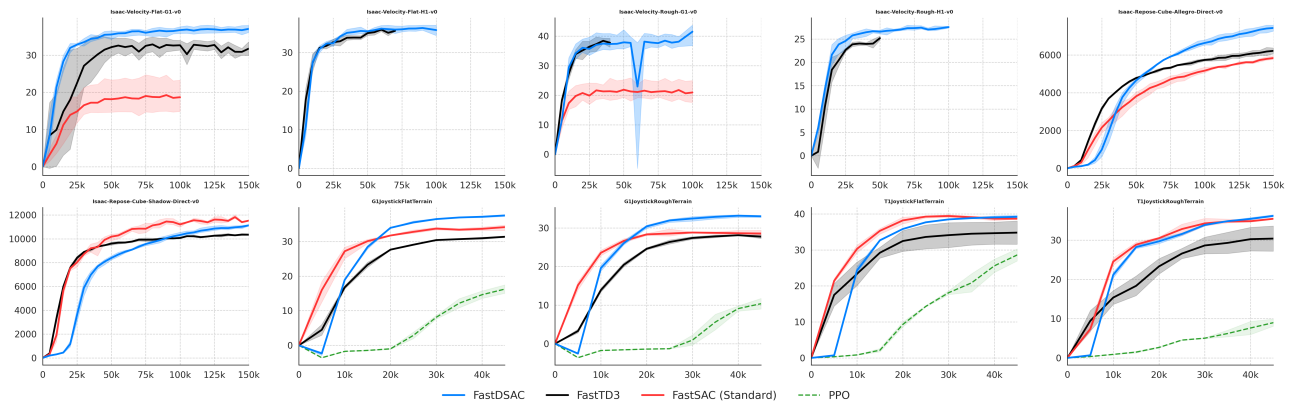


Figure 11. **Full Results on IsaacLab and MuJoCo Playground.** Learning curves for FastDSAC (blue), FastTD3 (black), FastSAC (Standard) (red), and PPO (green) across 10 diverse tasks. Top Rows (IsaacLab): FastDSAC demonstrates superior performance on locomotion tasks (Velocity Flat/Rough H1/G1) and manipulation tasks (Repose Cube Allegro), while remaining competitive on Repose Cube Shadow. Bottom Row (MuJoCo Playground): FastDSAC consistently outperforms baselines on high-dimensional humanoid control tasks (G1/T1 Joystick), exhibiting lower variance and higher asymptotic returns. Shaded regions denote min-max range across 3 seeds.